Liquid Crystals
Publication details, including instructions for authors and subscription information:
http://www.informaworld.com/smpp/title~content=t713926090

Synthesis and mesomorphic properties of a new chiral series with anticlinic and TGB phases

C. Da Cruz[a]; J. C. Rouillon[a]; J. P. Marcerou[a]; N. Isaert[b]; H. T. Nguyen[a]
[a] Centre de Recherche Paul Pascal, Avenue A. Schweitzer, F-33600 Pessac, France, [b] Laboratoire de Dynamique et Structure de Matériaux Moléculaires, Universitéde Lille 1, UFR de Physique, F-59655 Villeneuve d'Ascq Cedex, France,

Online publication date: 06 August 2010

To cite this Article Da Cruz, C. , Rouillon, J. C. , Marcerou, J. P. , Isaert, N. and Nguyen, H. T.(2001) 'Synthesis and mesomorphic properties of a new chiral series with anticlinic and TGB phases', Liquid Crystals, 28: 1, 125 — 137
To link to this Article: DOI: 10.1080/026782901462463
URL: http://dx.doi.org/10.1080/026782901462463

LIQUID CRYSTALS, 2001, VOL. 28, NO. 1, 125–137

Synthesis and mesomorphic properties of a new chiral series with anticlinic and TGB phases

C. DA CRUZ, J. C. ROUILLON, J. P. MARCEROU, N. ISAERT† and H. T. NGUYEN*

Centre de Recherche Paul Pascal, Avenue A. Schweitzer, F-33600 Pessac, France
†Laboratoire de Dynamique et Structure de Matériaux Moléculaires, Université de Lille 1, UFR de Physique, F-59655 Villeneuve d'Ascq Cedex, France

(*Received 14 February 2000; in final form 16 May 2000; accepted 28 May 2000*)

A series of difluoro substituted benzoate derivatives: (*R*)-1-methylheptyl 4-[4-(3-fluoro-4-alkyloxybenzoyloxy)-3-fluorobenzoyloxy]benzoates is reported. The short chain members ($n = 8$ to 10) display a very rich polymesomorphic sequence with anticlinic properties: Cr–SmC^*_A–SmC^*_{FI}–SmC*–SmC^*_α–SmA–I; the longer chain members exhibit only TGB and SmC* phases. The mesomorphic properties were studied by optical microscopy, DSC, X-ray diffraction, electro-optical and helical pitch measurements, and optical rotatory power studies. The effect of the number and position of fluorines on the mesomorphic sequence is discussed.

1. Introduction

A few years ago, chiral liquid crystals were paid much attention as a result of the experimental discovery of the twist grain boundary phase (TGB) by Goodby *et al.* [1] in 1989 and the anticlinic smectic C phase, initially called SmO*, by Levelut *et al.* in 1983 [2] and then the SmC^*_A phase by Chandani *et al.* in 1989 [3]. While the study of the twist grain boundary phase seems to be of academic interest, the SmC^*_A phase has been exploited for various device applications. Therefore, many compounds possessing this last phase have been synthesized, and Fukuda *et al.* mentioned in a review [4] that there are more than 300 pure compounds which display these properties.

Generally, the SmC^*_A phase is accompanied by other subphases (called subphases on account of their disappearance in racemic mixtures) such as the SmC^*_α and the ferrielectric phases. The SmC^*_A phase structure is now well established by resonant X-ray scattering studies [5], whereas the number and the structures of the ferrielectric phases are not too clear. For these reasons, the search for new materials is always welcome.

Whilst the molecular structures of compounds which exhibit SmC^*_A or TGBA phases are very close, they differ in their local dipolar moment. For example in the following series

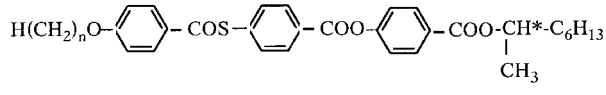

I

SmC^*_A and several SmC* phases are obtained, but the TGB phase is not observed for all chain lengths [6]. The determining parameter for the 'anticlinic series' is the local dipole moment of the COO group between the two phenyl groups near the chiral chain. On the other hand the tolane series

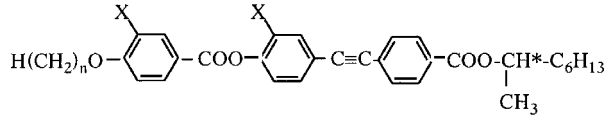

II

exhibits TGB phases when X = H, whereas when X = F the existence not only of this phase with a small helical pitch, but also of the new blue smectic phases (or TGB Blue phases) [7] is mentioned. So the presence of the two fluorines gives rise to the particular feature of a small helical pitch. Keeping this in mind we have introduced two such fluorines into an 'anticlinic series' in order to study their influence on the phase sequence and

*Author for correspondence; e-mail: tinh@arpp.u-bordeaux.fr

Liquid Crystals ISSN 0267-8292 print/ISSN 1366-5855 online © 2001 Taylor & Francis Ltd
http://www.tandf.co.uk/journals

the relationship between chemical structure and liquid crystalline properties. We would like to note that there are only a few series which display both TGB and SmC^*_A phases [1, 8, 9]. In most of these series that exhibit both phases, the TGB phase is present in the majority of the homologues, whereas the SmC^*_A phase is found only in a small number of them.

In this paper therefore we report the existence of SmC^*_A and TGB phases in the same series, and discuss the role and the position of the two fluorines. The new series has the general formula:

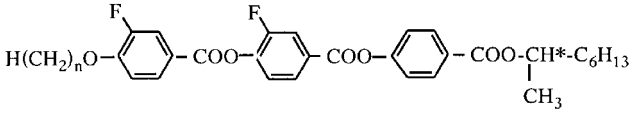

III

where $n = 7$–20.

2. Synthesis and mesomorphic properties

The compounds of the series were prepared following the pathway shown in the scheme. Details of the synthesis are reported in the experimental section. The preparation of the substituted benzoic acids used in the final esterification and of compounds **1**, **2**, **3**, and **4** has been described elsewhere [10, 11]. The final compounds were obtained by a classical esterification reaction between the chiral phenol and the various 4-alkoxy-3-fluorobenzoic acids [11].

All the compounds are mesomorphic. The phase behaviour and transition temperatures of the series members were determined both by thermal microscopy (Mettler FP5) and differential scanning calorimetry (Perkin-Elmer DSC 7). The liquid crystal transition temperatures and enthalpies for these new materials are summarized in the table and figure 1. Heating and cooling rates were 5°C min^{-1}. When transition enthalpies were too weak to be detected the temperatures given are those observed by polarizing optical microscopy.

For $n = 8$ and $n = 9$ we have the phase sequence Cr–SmC^*_A–SmC^*_{FI}–SmC*–SmC^*_α–SmA–I. However, we detect SmC^*_α phase only by DSC measurements; it is not detectable by microscopic observation because its texture is too similar to that of the SmA phase. The $n = 10$ member has the same phase sequence, but the SmC^*_α phase is not detected by DSC. Its existence is proved by helical pitch measurement and electro-optical studies (see next section). It disappears from $n = 11$.

Concerning the SmC^*_{FI} phases, there are in fact two phases which are not distinguished by DSC measurements, but are observed by microscopy. The temperature of transition between the two phases is difficult to determine, and in the table we indicate only the transition temperature between SmC^*_A and SmC^*_{FI1} determined by DSC. The presence of the two phases is confirmed by optical rotatory power measurements.

From $n = 13$ to $n = 18$ a TGB phase appears, whereas the ferrielectric and anticlinic phases disappear.

Table. Transition temperatures (°C) and enthalpies (given in italic in kJ mol^{-1}) of the series.

n	Cr		SmC^*_A		SmC^*_{FI} 1 and 2		SmC*		SmC^*_α		SmA		TGBA		I
7	•	68.5					•	70.4			•	108			•
		17.94						*0.081*				*4.993*			
8	•	61.9	•	67.5	•	69.4	•	79.5	•	80.8	•	106.7			•
		23.67		*0.009*		*0.010*				*0.101*		*4.976*			
9	•	65.2	•	69.5	•	75.7	•	90	•	90.8	•	103.6			•
		37.67		*0.008*		*0.014*				*0.263*		*4.698*			
10	•	57.7	•	80.6	•	83.5	•	93.9	•	94.5	•	103.7			•
		31.80		*0.02*		*0.02*		*0.272*				*4.966*			
11	•	69.3	•	(44.2)	•	(56.5)	•	95.3			•	101.7			•
		35.19						*0.359*				*4.961*			
12	•	67.9	•	(61.1)	•	72.4	•	97.1			•	101.5			•
		33.68				*0.010*		*0.331*				*5.053*			
13	•	62.9					•	96.8					•	100	•
		31.79						*0.367*						*4.673*	
14	•	54.7					•	98.5					•	101.3	•
		32.74						*0.358*						*4.948*	
16	•	52.1					•	94.6					•	97	•
		29.16												*5.582*	
18	•	50.6					•	93.7					•	96.6	•
		31.28						*0.234*						*5.002*	
20	•	58.6					•	83.7					•	89.3	•
		58.96						*0.180*						*4.594*	

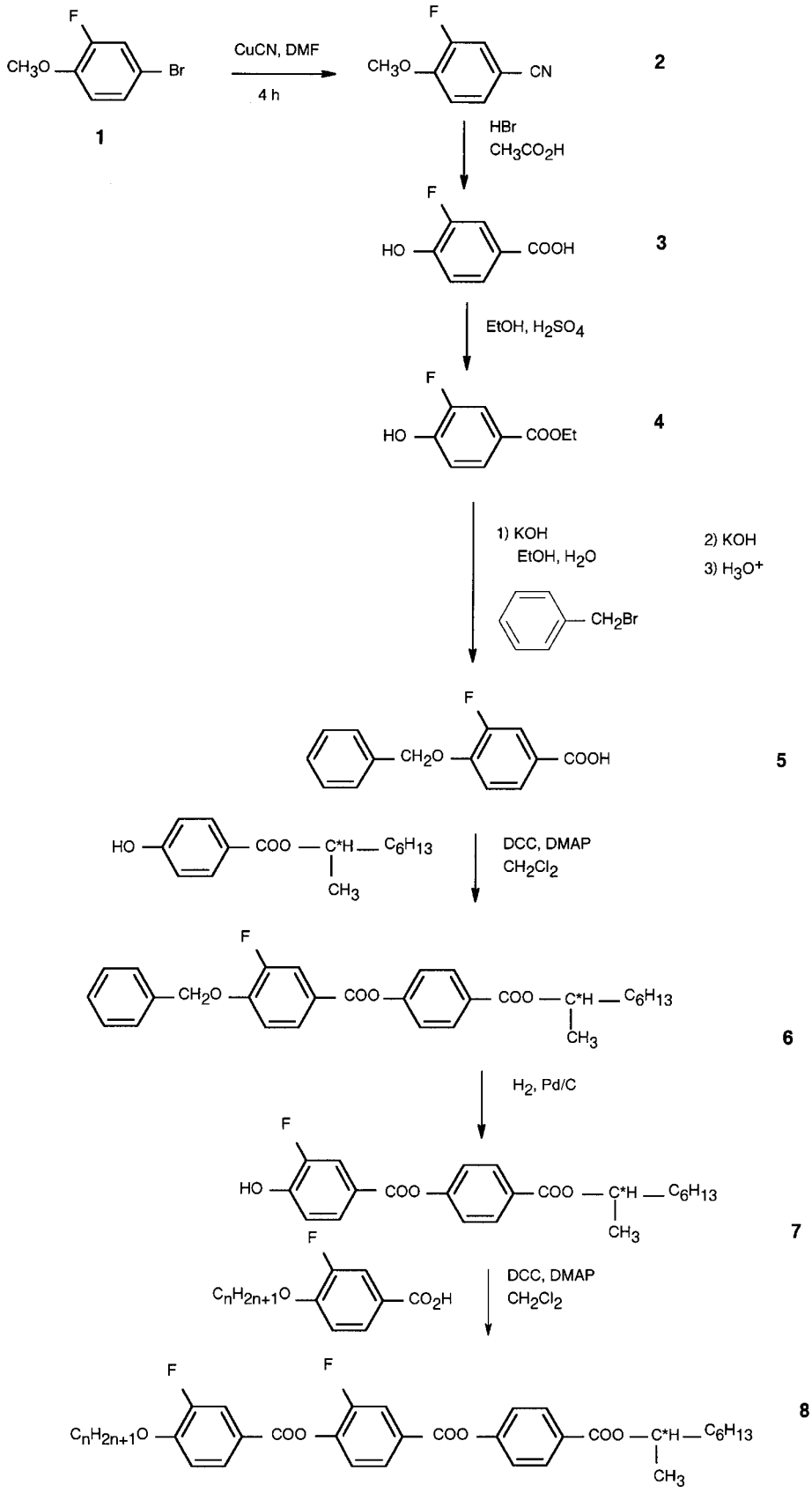

Scheme.

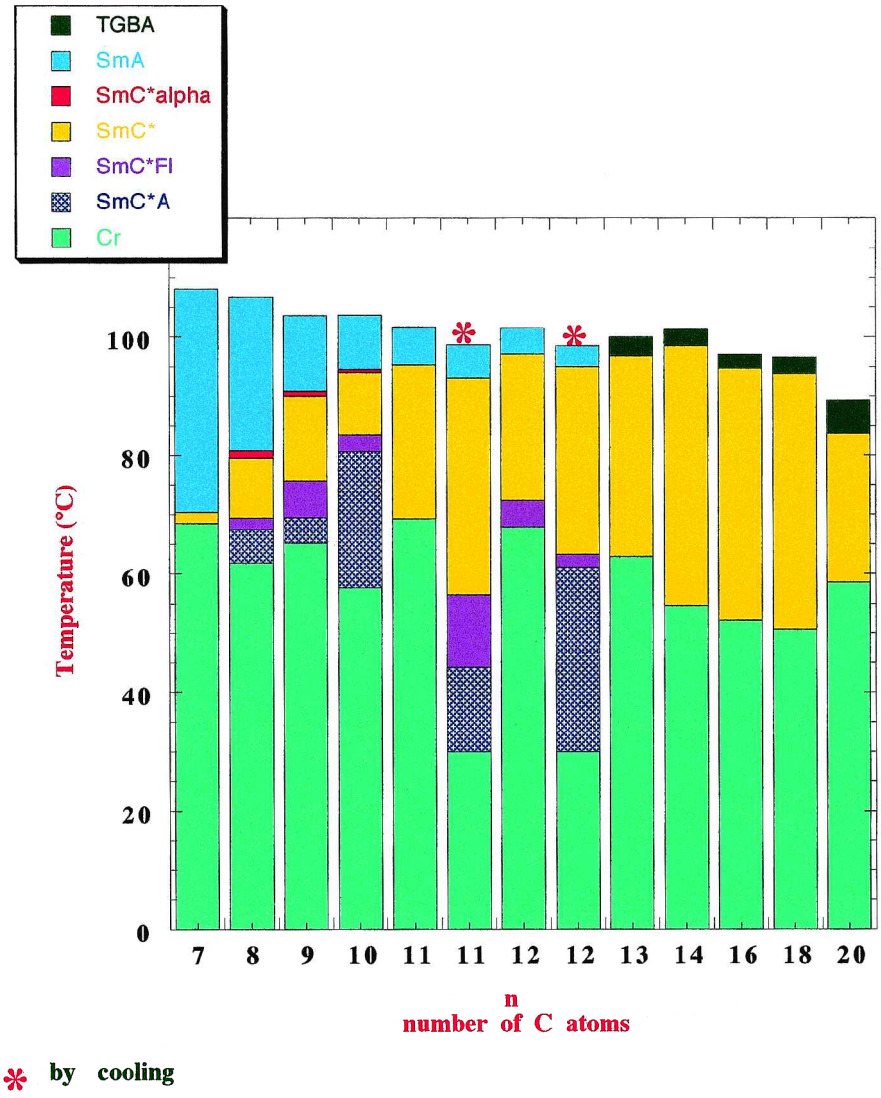

Figure 1. Plot of transition temperatures (°C) versus number of C atoms.

If we take the example of compound $n = 10$, on cooling from the isotropic liquid, homeotropic and focal-conic textures of the SmA phase first appear, figure 2(*a*). Then the ferroelectric phase (SmC*) is obtained with striated fan-shaped and coloured pseudo-homeotropic textures, figure 2(*b*). On further cooling, the ferrielectric (SmC^*_{FI}) phase arrives with a typical texture given in the previously homeotropic parts of the cell, figure 2(*c*): the texture constantly moves, due to helical pitch or domain changes. The second ferrielectric phase moves considerably less than the first and persists for approximately 2.5°C. Further cooling gives the anticlinic phase which is similar in appearance to a ferroelectric phase and very coloured, figure 2(*d*).

For the compounds with a long terminal chain ($n = 13$ to 18), we observed the TGB phase with filamentous textures on heating from SmC* phase with homeotropic alignment or with developing domains and planar cholesteric-like textures on cooling from the isotropic phase, figure 3. Let us point out that:

(1) The SmA–I and TGBA–I transition enthalpies in this series are constant (about 5 kJ mol^{-1}), while in other TGB series they decrease with chain length. This behaviour seems to be correlated with the presence of the so-called 'antiferroelectric' phases in the series under study.

(2) The $n = 11$ derivative displays monotropic SmC^*_A and SmC^*_{FI} phases with temperatures that are quite different from the others. This behaviour is not due to the purity of the material (we have checked the purity); perhaps it is related to the high melting point.

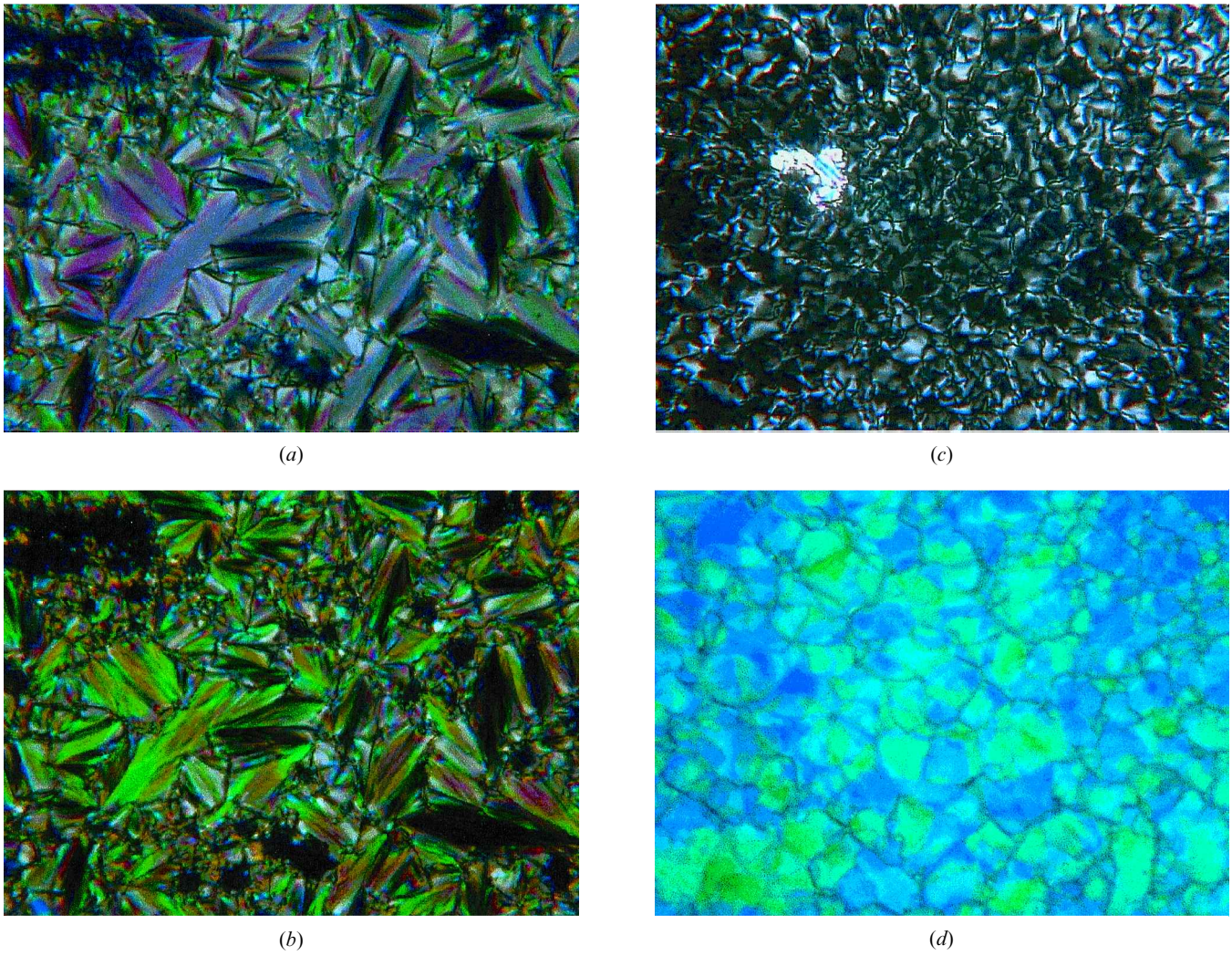

Figure 2. Optical textures of smectic phases for $n = 9$: (*a*) SmA phase at 95°C; (*b*) SmC* phase at 90.5°C; (*c*) SmC^*_{FI} phase at 66°C; (*d*) SmC^*_A phase at 59°C.

3. Electro-optical studies

Electro-optical properties were studied using the SSFLC configuration to evaluate polarization, response time, and tilt angle in a single set-up. Commercial cells (EHC from Japan) coated with ITO (indium tin oxide) and rubbed polyimide were used. The thickness of the cells was 15 μm, and the active area was 0.25 cm^2. Slow cooling through the isotropic to SmA phase transition (at 0.1°C min^{-1}) leads to planar alignment. The compound with $n = 10$ was studied, and the measurements were done upon cooling to facilitate the alignment.

The polarization is calculated by integration of the switching current under a rectangular a.c. field at 30 Hz. The field value is 4 V μm^{-1}, such a field being sufficient to unwind the helical structure and accomplish the phase transition from SmC^*_A, SmC^*_{FI}, SmC* and SmC^*_α phases to the unwound SmC* phase. As pictured in figure 4, the polarization versus temperature showed no anomalies at the phase transition temperatures. The values of the saturated polarizations are quite high, as observed for many three-ring compounds. The plateau value is more than 130 nC cm^{-2}.

A square wave voltage of 4 V μm^{-1} was used for the response time measurements. The electric response time is the time required for the majority of the molecules to switch under the applied field. Obviously the electric response time decreases with increasing temperature and changes from 56.3 μs at $T = 70$°C to 14.6 μs at $T = 95$°C (figure 5).

The apparent tilt angle θ of the molecules from the smectic layer normal was calculated from the difference between the extinction positions of the sample between crossed polarizers under a rectangular a.c. field (4 V μm^{-1}) at very low frequency (0.2 Hz). The accuracy

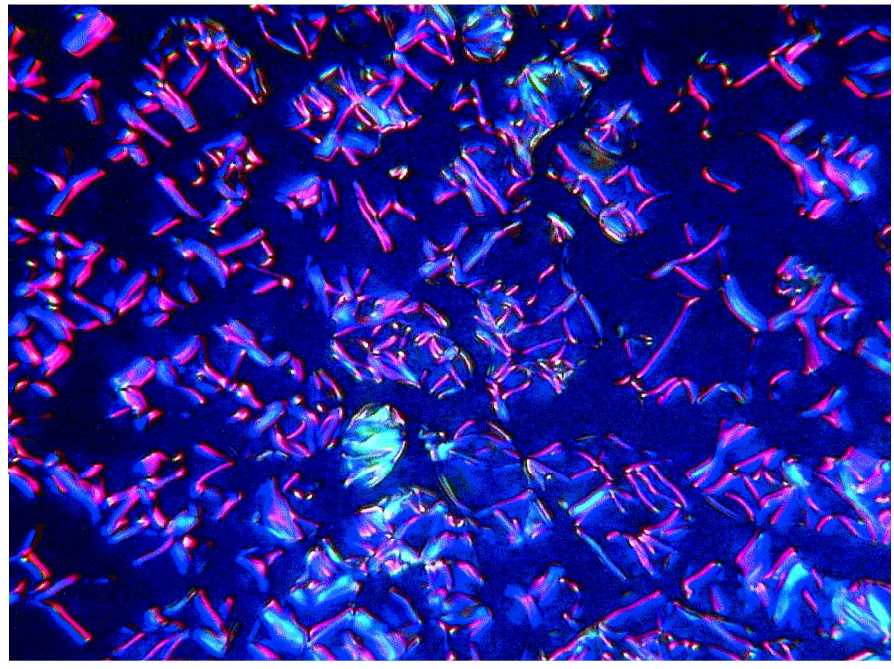

Figure 3. Optical texture of TGBA phase of the compound $n = 13$ at 96°C.

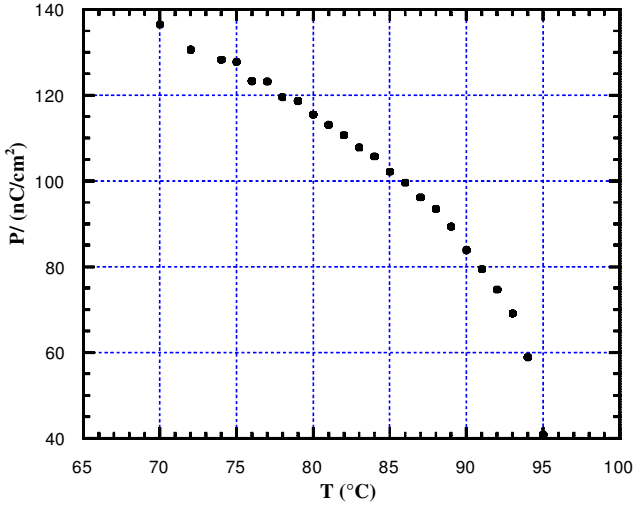

Figure 4. Temperature dependence of the polarization at saturation ($E = 4$ V μm^{-1}) for $n = 10$.

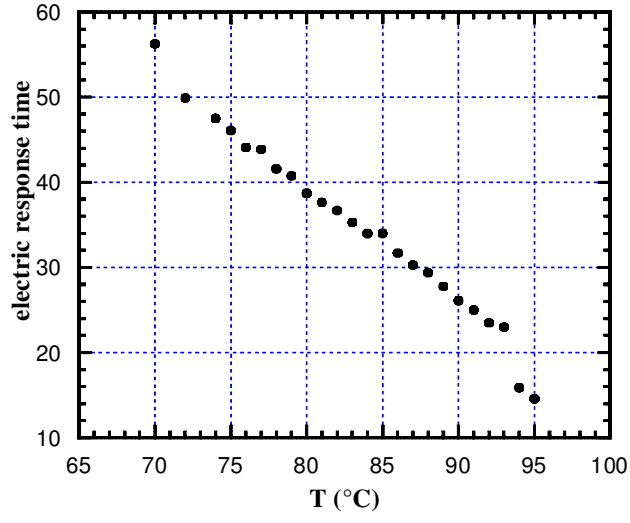

Figure 5. Temperature dependence of the the electric response time (μs) at saturation ($E = 4$ V μm^{-1}) for $n = 10$.

of the measurement was estimated as $\pm 1°$ (figure 6). As for the polarization, tilt angle versus temperature showed no anomalies at the phase transition temperatures. Its value reached about 30°.

We also used special waveforms truncated at voltages $-V$, 0 and $+V$, see figure 7 (*a–d*). This allows for example the recognition of the smectic C^*_α phase from the smectic C* phase when there is some ambiguity. One sees in figures 7 (*a*) and 7 (*b*) that in the smectic C* phase, below a threshold of about 10 V/15 μm, the macroscopic helix rewinds each time the voltage vanishes, while above the threshold, one reaches bistable behaviour without helix. On the contrary, in the smectic C^*_α phase, whatever the amplitude of the maximum applied voltage, there is a phase transition between the induced smectic C* and the zero field smectic C^*_α.

4. X-ray measurements

X-ray diffraction experiments were performed to determine the layer thickness of the different lamellar phases; only the $n = 10$ compound was studied. The molecular length in the extended configuration of the $n = 10$ derivative is 46 Å and the layer thickness is about 38 Å in the SmA phase. The low value of the layer

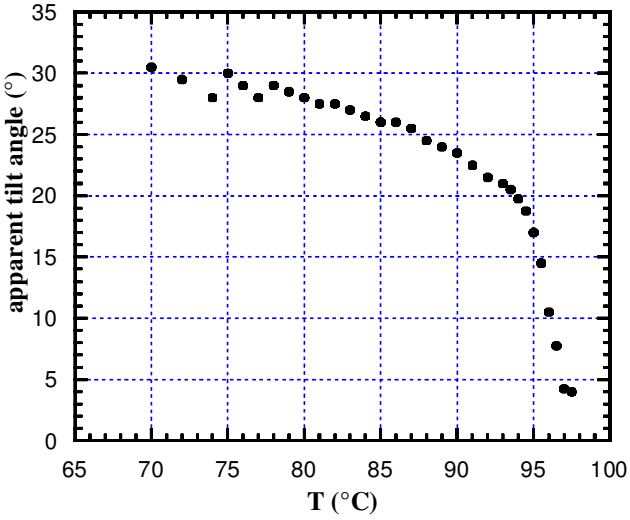

Figure 6. Temperature dependence of the apparent tilt angle ($E = 4$ V μm^{-1}) for $n = 10$.

spacing with regard to the molecular length suggests that there is an interpenetration of the chains in the layer or that the core parts of the molecules are already tilted in the SmA phase [12]. The layer spacing decreases abruptly at the SmA–SmC$^*_\alpha$ transition indicating the tilted character of the SmC$^*_\alpha$ phase. Then the layer spacing decreases regularly on cooling throughout the SmC*, SmC$^*_{FI}$ and SmC$^*_A$ phases. Let us point out however that the decrease of the layer thickness is stepped in nature in the SmC$^*_{FI}$ phase (figure 8). This behaviour is similar to that obtained with the tolane series [13].

5. Helical pitch measurements

We performed pitch measuements on the SmC$^*_A$, SmC* and TGBA phases, and optical period measurements on the SmC$^*_\alpha$ phase. We used the Grandjean–Cano method for the TGBA phase in the planar orientation and for the SmC* and SmC$^*_A$ phases in the homeotropic orientation. We also used the free surface homeotropic drop method for the SmC$^*_\alpha$ and SmC* phases. Both methods have already been described [14, 15]. Period variations are displayed in figures 9, 10.

5.1. $n = 9$

In the SmC$^*_A$ phase, the pitch is about $p \cong 0.34$ μm and does not significantly vary; this value is in keeping with the selective reflection colour: green–blue ($\lambda \cong np$).

In the SmC* phase, the pitch is about 0.24 μm over a wide temperature range; it is short enough to give selective reflexion of visible light with $\lambda = 2np$; this phase is dark red. At high temperatures the pitch is about 0.22 μm (87°C) and suddenly falls to 0.13 μm at 89°C; the compound reflects $\lambda = 2np$ giving orange, green, violet light as p decreases.

The SmC$^*_\alpha$ phase exists over about 1°C. Very flat homeotropic drops observed with reflected light exhibit Friedel fringes due to periodic variations of the light ellipticity. These fringes can be compared to wedge fringes corresponding to a thickness variation of about 0.18 μm ($\lambda/2n$). Figure 10 displays the double period versus temperature trend generally observed on heating: the period rapidly varies from 0.13 μm (the pitch of the SmC* phase at 89°C), to 0.06 μm at 90°C (at 90°C the fringes freeze, indicating the transition to SmA). Two photographs of the sample are given in figure 11. Different behaviours can be observed on cooling. The most common one is quasi-reversible, with values increasing from 0.06 to 0.13 μm. But sometimes the variation is different: the observed period first diverges, and then converges to 0.13 μm. Such surprising behaviour is a common feature of SmC$^*_\alpha$ phases [15, 16].

5.2. $n = 10$

Results obtained for $n = 10$ are similar to those for $n = 9$: $p \cong 0.32$ μm for the dark blue SmC$^*_A$ phase; $p \cong 0.25$ μm for the dark red SmC* phase; the pitch falls to 0.13 μm near the SmC*–SmC$^*_\alpha$ transition. The period in the SmC$^*_\alpha$ phase varies from 0.13 μm to 0.06 μm; this phase has a shorter temperature range (0.7°C).

5.3. $n = 14$

The SmC* phase can be supercooled to room temperature; then $p \cong 0.25$ μm and the compound reflects both violet (np) and red ($2np$) colours. The pitch slowly increases: $p \cong 0.28$ μm at 50°C, 0.31 μm at 94°C; in this interval the liquid crystal is violet to blue–violet ($\lambda = np$). A sudden decrease of the pitch occurs between 95 and 96.2°C; the compound reflects red, orange, green, blue and violet light ($2np$) as p decreases to 0.13 μm. We can easily verify the absence of the SmC$^*_\alpha$ phase: very flat homeotropic drops show, just after the violet colour, Friedel fringes with a double period $p \cong 0.12$ μm; these fringes immediately freeze, indicating a direct SmC*–SmA transition.

TGBA exists over a short temperature range (≈ 3°C) between SmC* and I. The focal-conic texture is obtained spontaneously on cooling the I phase of the compound mounted between two glasses (figure 12); the helical axes are then distributed in all directions in the sample plane. At higher temperatures, the focal domains are finely streaked, but at lower temperatures, the streaks become wider and wider, showing that the helical pitch increases on cooling. The Grandjean–Cano texture can also be obtained (figure 13), with much difficulty; this allowed us to evaluate the helical pitch at 1 μm near the I phase and 1.1 μm 0.5°C below this. We have not been able to

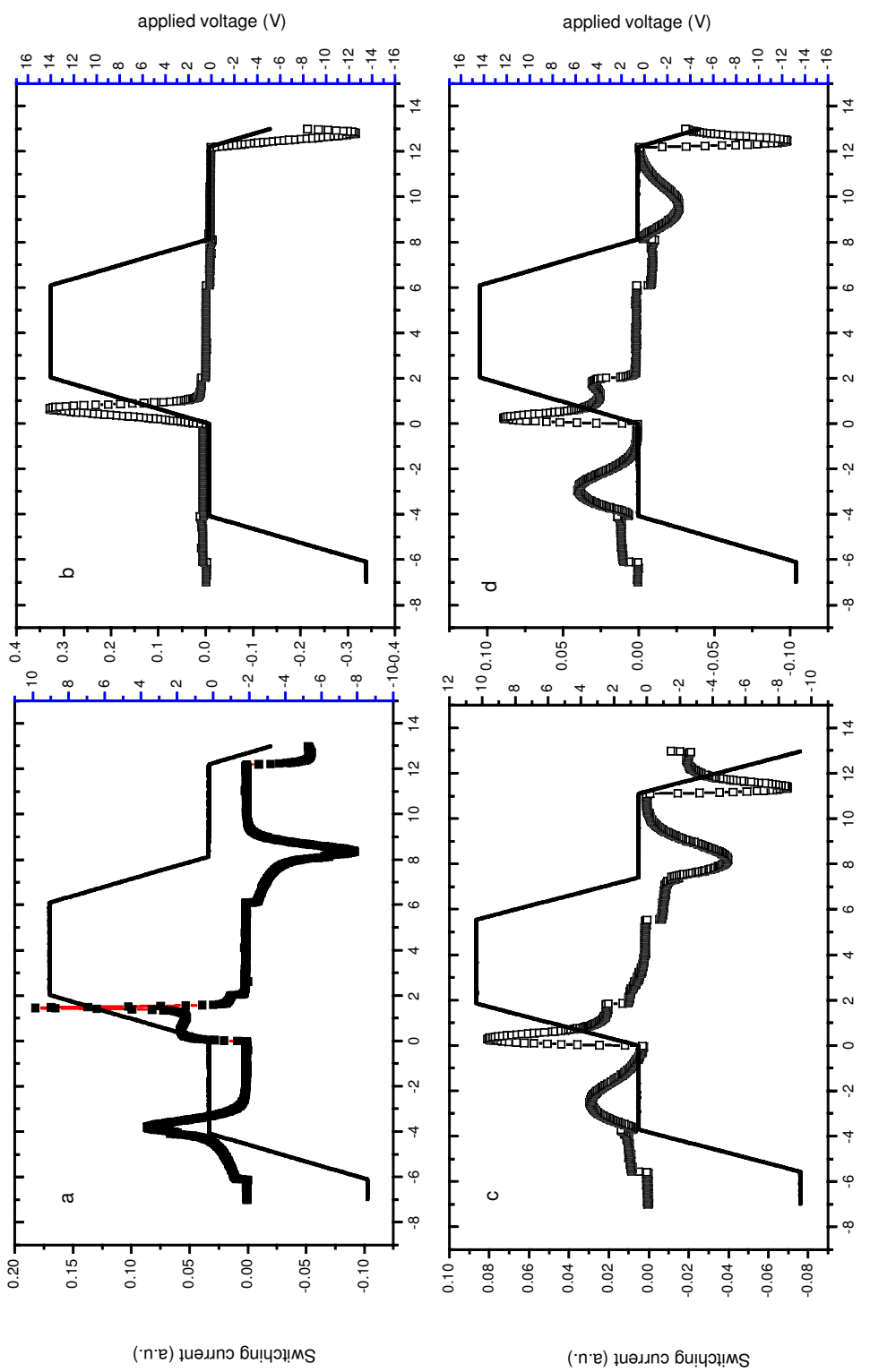

Figure 7. Switching current for the SmC* and SmC^*_α phases at different fields: (*a*) helix rewinding in SmC* at 9 V/15 µm; (*b*) unwound SmC* at 14 V/15 µm; (*c*) at 9 V/15 µm; (*d*) at 14 V/15 µm—phase transitions back and forth from SmC* to SmC^*_α.

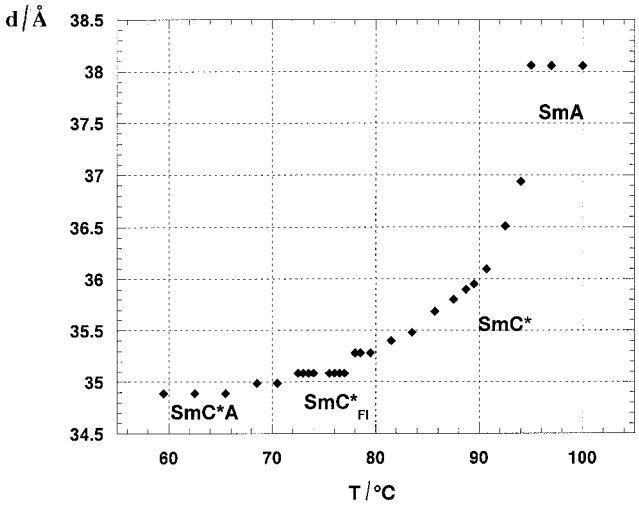

Figure 8. Layer spacings of different smectic phases.

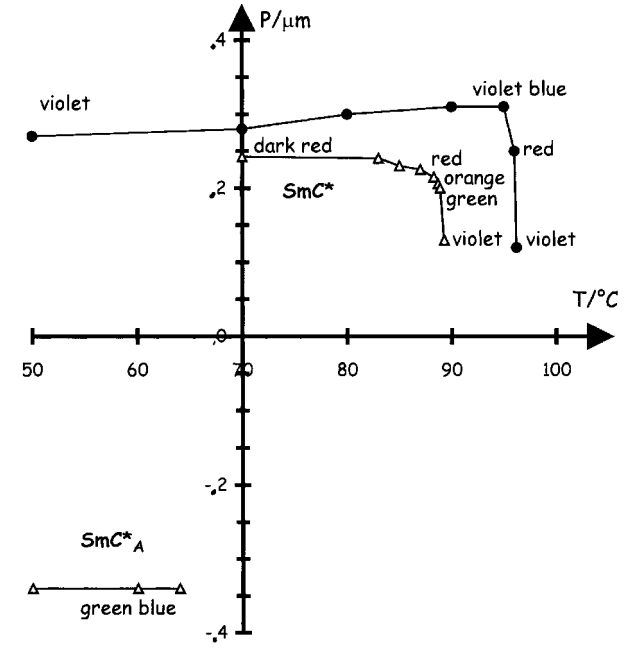

Figure 9. Helical pitch versus temperature in the SmC* and SmC^*_A phases for compounds $n = 9$ (△) and $n = 14$ (●).

measure accurately the pitch increase at lower temperatures: high viscosity and anchoring effects did not allow the sample to unwind easily.

On heating the SmC* phase with a focal-conic texture, the focal-conic SmA phase first appears; then, just before the I phase, a Grandjean–Cano texture forms. In a similar way, the homeotropic SmC* phase transforms into a homeotropic SmA in which filaments develop; these filaments are compact in rather thick samples, and sparse in thin samples. These observations do not prove the existence of any SmA phase; they only show that surface effects can easily unwind the TGBA phase.

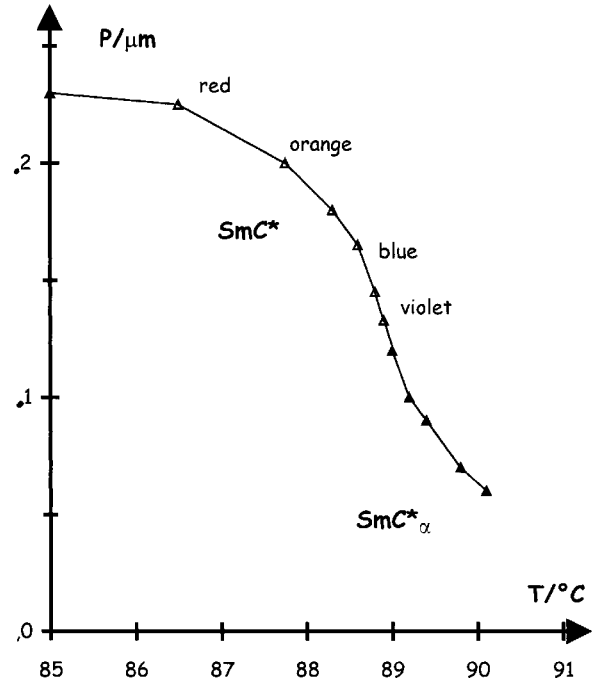

Figure 10. Helical pitch in the SmC* phase (△) and double optical period in the SmC^*_α phase (▲) for compound $n = 9$.

6. Optical rotatory power measurements

Measurement of the optical rotatory power (ORP) was done in a 100 μm thick, homogeneously aligned cell illuminated by a HeNe laser beam at 632.8 nm. The result is the now classical one for chiral compounds presenting the whole phase sequence of tilted smectics with very low pitch. The compound under study was the $n = 10$ (R) enantiomer which shows a negative and small ORP in the smectic C* phase, vanishing towards the smectic C^*_α phase due to the simultaneous decrease of the tilt angle and the pitch value (figure 14). The sign is characteristic of a compound with a left handed pitch smaller than the light wavelength λ/n inside the sample, according to the classical formula of deVries. At a lower temperature, one reaches the $SmC^*_{FI_2}$ phase with the same helix handedness, but a much higher pitch value. Then on cooling one enters the smectic $SmC^*_{FI_1}$ phase with the opposite right handedness and a large pitch. Finally one recovers the anticlinic phase with a small pitch.

7. Discussion and conclusion

It is well known that the usual molecular structures of compounds which display TGB and SmC^*_A phases are very similar and that they only differ in the dipole moment of the linking group between two phenyl groups near the chiral centre. For example in the following series, when the bridge X is a symmetric non-polar

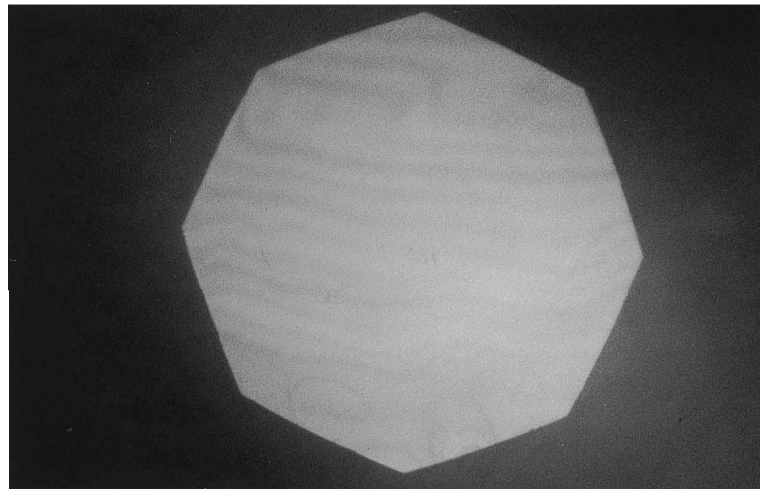

(*a*)

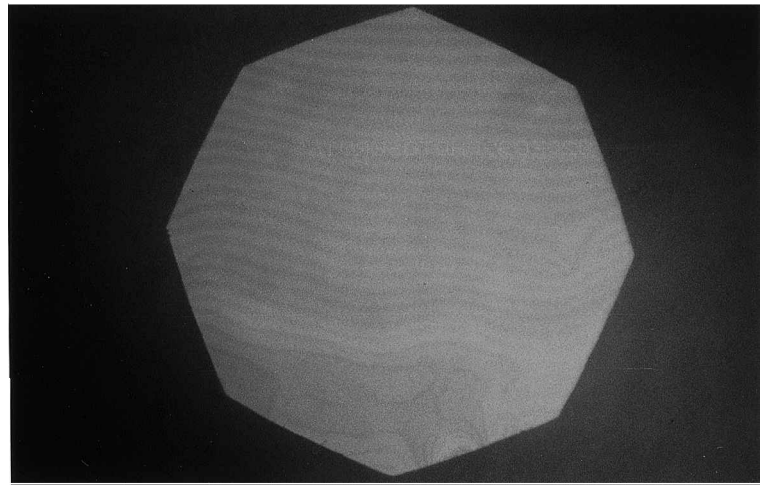

(*b*)

Figure 11. Friedel fringes on a flat homeotropic drop of $n = 9$: (*a*) with $p = 0.12\,\mu m$; (*b*) with $p = 0.06\,\mu m$.

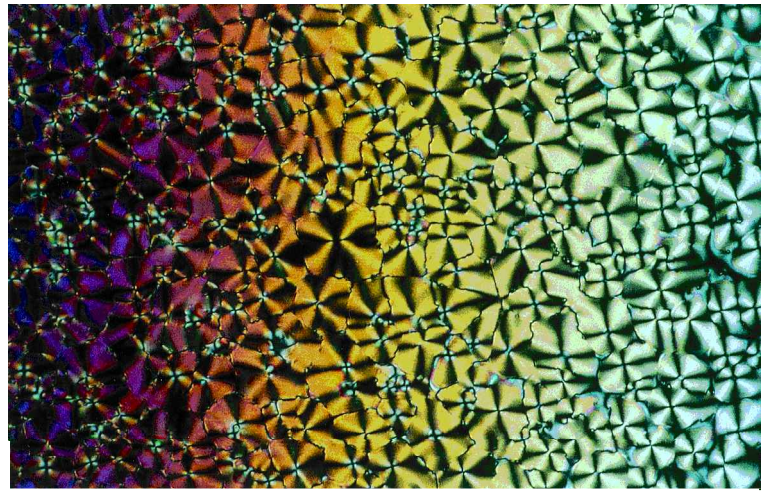

Figure 12. TGBA phase with focal-conic texture for $n = 14$ at 98°C.

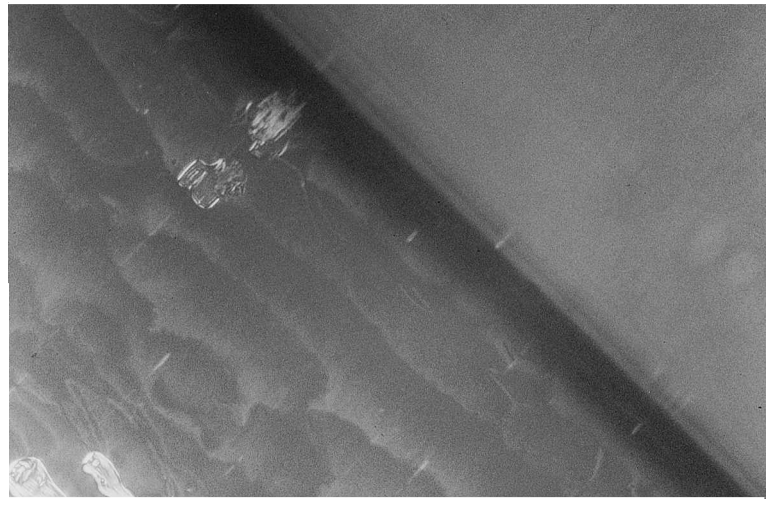

Figure 13. TGBA phase with Grandjean–Cano texture for $n = 14$ at 98°C.

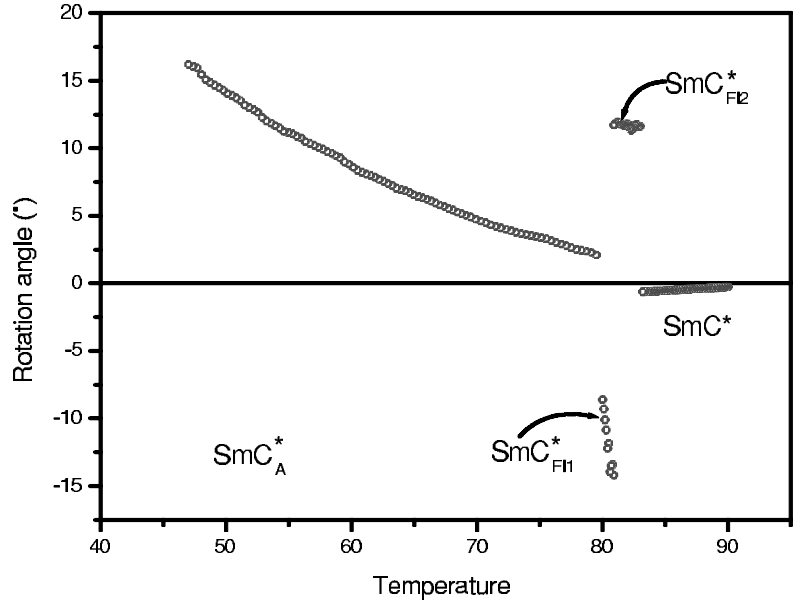

Figure 14. Optical rotation at 632.8 nm in a 100 µm thick homeotropic sample of the $n = 10$ compound.

group such as −N=N−, −CH=CH−, −C≡C− or a single bond, the TGB phase is almost always observed

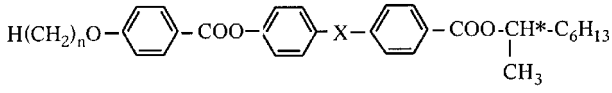

IV

On the other hand, when X is a polar group such as −COO− or −COS−, the molecules having the following structure:

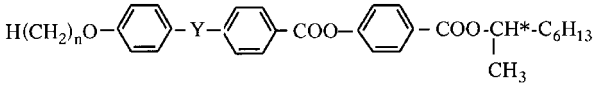

V

they generally display the anticlinic behaviour (with Y = −, −C≡C−, −N=N−, −COS−, −COO−).

Only the influence of the number and the position of fluorine substituents on the first phenyl ring (near the aliphatic chain) on the mesomorphic sequence (TGB or SmC^*_A phases) has been studied [17–18]. A slight change between these two phases was demonstrated. Recently Li *et al.* [7] reported the TGB series **II** which displays smectic blue phases, TGB and SmC* phases with short helical pitch. Therefore we applied this result to the 'anticlinic series' **III** in the hope that the short pitch of the SmC* could twist the SmA phase. Figure 9 shows clearly that the helical pitch of the SmC* for $n = 9$ and $n = 14$ is lower than 0.3 µm, while the unfluorinated or monofluoro substituted materials exhibit SmC* phases with a pitch about 0.4 µm [17–19]. The existence of the TGB phase in an 'anticlinic series' gives us hope of obtaining the TGB phase with anticlinic properties.

Furthermore, the polarization at saturation (4 V μm^{-1})

for $n = 10$ is nearly 140 nC cm^{-2}, higher than that of the unfluorinated or monofluoro substituted homologues (lower than 100 nC cm^{-2}) [19].

8. Experimental

NMR spectra were recorded on a Bruker HW 200 MHz spectrometer. Infrared spectra were recorded on a Perkin-Elmer 783 spectrophotometer. The following examples are typical of the synthetic methods used to obtain the compounds given in the table.

8.1. *4-Benzyloxy-3-fluorobenzoic acid (**5**)

To a solution of KOH (4.2 g, 0.0075 mol), water (10 ml), ethanol (50 ml) and ethyl 4-hydroxy-3-fluorobenzoate **4** (9.2 g, 0.05 mol) was added dropwise benzyl bromide (6.5 ml, 0.055 mol). The mixture was stirred under reflux for 3 h. After cooling to room temperature, KOH (3.5 g, 0.0625 mol) in water (10 ml) was added and the mixture once again stirred under reflux for 2 h. After cooling, the solvent was evaporated and then concentrated HCl (12 ml) and water (100 ml) were added. The mixture was stirred for 30 min and the solid filtered off, washed with water and crystallized from ethanol; yield 9.2 g (74.4%). ^{1}H NMR ($CDCl_3$, ppm): 5.2 (s, 2H, $-CH_2-O-$), 7.1 (t, 1H arom. *meta* to F), 7.4 (m, 5H arom.), 7.8 (m, 2H, *ortho* and *para* to F). IR (KBr) (cm^{-1}): large signal 2950 (O–H), 1680 (C=O), 1617, 1518, 1450 (C=C phenyl rings).

8.2. *(*R*)-1-Methylheptyl 4-(4-benzyloxy-3-fluorobenzoyloxy)benzoate (**6**)

To a solution of (*R*)-1-methylheptyl 4-hydroxybenzoate in CH_2Cl_2 was added DCC (6 g, 0.026 mol), DMAP (0.26 g, 0.026 mol) and compound **5** (6.4 g, 0.026 mol). The mixture was stirred at room temperature overnight, the solid filtered off, the solvent evaporated and the residue purified by chromatography on silica gel using CH_2Cl_2 as eluent; yield 8.7 g (70%). ^{1}H NMR ($CDCl_3$, ppm): 0.9 (t, 3H, CH_3 of C_6H_{13}), 1.2–1.5 (m, 11H, $4CH_2$ and CH_3-CHO), 1.6–1.8 (m, 2H, $\underline{CH_2}-CHO$), 5.15 (m, 1H, $O-\underline{CH}-CH_2-$) 5.2 (s, 2H, $-CH_2-O-$), 7.1 (t, 1H arom. *meta* to F), 7.3 (d, 2H, arom.), 7.4 (m, 5H arom.), 7.9 (m, 2H, *ortho* and *para* to F), 8.1 (d, 2H, arom.). IR (KBr) (cm^{-1}): 2958, 2927, 2858 (C–H aliphatic), 1716 (C=O), 1618, 1526, 1440 (C=C phenyl rings), 936 (*para*).

8.3. *(*R*)-1-Methylheptyl 4-(4-hydroxy-3-fluorobenzoyloxy)benzoate (**7**)

To a solution of compound **6** (8 g, 0.017 mol) in about 200 ml of ethyl acetate was added 1 g of catalyst (Pd/C). Hydrogen was added under slight pressure. When the reaction was finished, the catalyst was filtered off and the solvent evaporated. As the reaction is quantitative, the liquid phenol was used without further purification; yield 6 g (91%). ^{1}H NMR ($CDCl_3$, ppm): 0.9 (t, 3H, CH_3 of C_6H_{13}), 1.2–1.5 (m, 11H, $4CH_2$ and CH_3-CHO), 1.6–1.8 (m, 2H, CH_2-CHO), 4.15 (m, 1H, OH), 5.15 (m, 1H, $O-\underline{CH}-CH_2-$), 7.1 (t, 1H arom. *meta* to F), 7.3 (d, 2H, arom.), 7.9 (m, 2H, *ortho* and *para* to F), 8.1 (d, 2H, arom.). IR (NaCl) (cm^{-1}): 3346 (O–H), 2956, 2932, 2859 (C–H aliphatic), 1740, 1716 (C=O), 1617, 1604, 1520, 1505, 1440, 1413 (C=C of the two phenyl rings), 931 (*para*).

8.4. *(*R*)-1-Methylheptyl 4[4-(4-decyloxy-3-fluorobenzoyloxy)-3-fluorobenzoyloxy]benzoate (*n* = 10) (**8**)

To a solution of phenol **7** (0.194 g, 0.5 mmol) in CH_2Cl_2 (5 ml) was added DCC (0.12 g, 0.5 mmol), DMAP (0.005 g, 0.5 mmol) and 4-decyloxy-3-fluorobenzoic acid (0.148 g, 0.5 mmol). The resulting mixture was stirred at room temperature overnight and then filtered; the solvent was evaporated from the filtrate. The residue was purified by chromatography on silica gel using CH_2Cl_2 as eluent. The product (a white powder) was crystallized from absolute ethanol; yield 0.2 g (60%). ^{1}H NMR ($CDCl_3$, ppm): 0.9 (t, 6H, CH_3 of C_6H_{13}, CH_3 of $C_{10}H_{21}$), 1.2–1.5 (m, 25H, $7CH_2$ of $C_{10}H_{21}$, $4CH_2$ and CH_3-CHO), 1.6–1.8 (m, 4H, $2CH_2\beta$), 5.15 (m, 1H, $O-\underline{CH}-CH_2-$), 7.1 (t, 1H arom. *meta* to F first ring), 7.25 (t, 1H arom. *meta* to F), 7.3 (d, 2H, arom.), 7.9 (m, 2H, *ortho* and *para* to F first ring), 8 (m, 2H, *ortho* and *para* to F), 8.1 (d, 2H, arom.). IR (KBr) (cm^{-1}): 2953, 2925, 2853 (C–H aliphatic), 1740, 1712 (C=O), 1615, 1513, 1439 (C=C phenyl rings).

The authors wish to thank Dr M. F. Achard for performing the X-ray diffraction measurements. C. Da Cruz wishes to thank Praxis XXI for financial support.

References

[1] Goodby, J. W., Waugh, M. A., Stein, S. M., Chin, E., Pindak, R., and Patel, J., 1989, *J. Am. chem. Soc.*, **111,** 8119.
[2] Levelut, A. M., Germain, C., Keller, P., Liebert, L., and Billard, J., 1983, *J. de Phys.*, **44,** 623.
[3] Chandani, A. D. L., Ouchi, Y., Takezoe, H., Fukuda, A., Furukawa, K., and Kichi, A., 1989, *Jpn. J. appl. Phys.*, **28,** 1261.
[4] Fukuda, A., Takanishi, Y., Isozaki, T., Ishikawa, K., and Takezoe, H., 1994, *J. mater. Chem.*, **4,** 997.
[5] Mach, P., Pindak, R., Levelut, A. M., Barois, P., Nguyen, H. T., Huang, C. C., and Furenlid, L., 1998, *Phys. Rev. Lett.*, **81,** 1015.
[6] Nguyen, H. T., Rouillon, J. C., Cluzeau, P., Sigaud, G., Destrade, C., and Isaert, N., 1994, *Liq. Cryst.*, **17,** 571.
[7] Li, M. H., Laux, V., Nguyen, H. T., Sigaud, G., Barois, P., and Isaert, N., 1997, *Liq. Cryst.*, **23,** 389.
[8] (*a*) Nguyen, H. T., Destrade, C., Parneix, J. P.,

Pochat, P., Isaert, N., and Girold, C., 1993, *Ferroelectrics*, **147,** 181; (*b*) Tuffin, R. P., Goodby, J. W., Bennemann, D., Heppke, G., Lotzsch, D., and Scherowsky, G., 1995, *Mol. Cryst. liq. Cryst*., **260,** 51.
[9] Navailles, L., Nguyen, H. T., Barois, P., Isaert, N., and Delord, P., 1996, *Liq. Cryst*., **20,** 653.
[10] Kelly, S. M., 1989, *Helv. Chim. Acta*, **72,** 594.
[11] Nabor, M. F., Nguyen, H. T., Destrade, C., Marcerou, J. P., and Twieg, R. J., 1991, *Liq. Cryst*., **10,** 785.
[12] Zgonik, M., Rey-Lafon, M., Destrade, C., Leon, C., and Nguyen, H. T., 1990, *J. Phys. Fr*., **51,** 2015.
[13] Cluzeau, P., Nguyen, H. T., Destrade, C., Isaert, N., Barois, P., and Babeau, A., 1995, *Mol. Cryst. liq. Cryst*., **260,** 69.
[14] Laux, V., Isaert, N., Joly, G., and Nguyen, H. T., 1999, *Liq. Cryst*., **26,** 361.
[15] Laux, V., Isaert, N., Faye, V., and Nguyen, H. T., 2000, *Liq. Cryst*., **27,** 81.
[16] Nguyen, H. T., Twieg, R. J., Nabor, M. F., Isaert, N., and Destrade, C., 1991, *Ferroelectrics*, **121,** 187.
[17] Nguyen, H. T., Babeau, A., Rouillon, J. C., Sigaud, G., Isaert, N., and Bougrioua, F., 1996, *Ferroelectrics*, **179,** 33.
[18] Faye, V., Rouillon, J. C., Destrade, C., and Nguyen, H. T., 1995, *Liq. Cryst*., **19,** 47.